Geophysical Journal International

Geophys. J. Int. (2020) **0**, 1–0 doi: 10.1093/gji/ggaa100

GJI Seismology

Green's function of the Lord–Shulman thermo-poroelasticity theory

Jia Wei,[1,5,7] Li-Yun Fu,[2,6] Zhi-Wei Wang,[1,5,7] Jing Ba[3] and José M. Carcione[4]

[1] *Key Laboratory of Earth and Planetary Physics, Institute of Geology and Geophysics, Chinese Academy of Sciences,* 19 *Beitucheng Western Road, Chaoyang District, Beijing* 100029*, China*

[2] *Laboratory for Marine Mineral Resources, Qingdao National Laboratory for Marine Science and Technology, Qingdao* 266071*, China. E-mail: lfu@upc.edu.cn*

[3] *School of Earth Sciences and Engineering, Hohai University, Nanjing* 211100*, China*

[4] *Istituto Nazionale di Oceanografia e di Geofisica Sperimentale (OGS), Borgo Grotta Gigante* 42c*, Sgonico, Trieste* 34010*, Italy*

[5] *University of Chinese Academy of Sciences, Beijing* 100049*, P. R. China*

[6] *Key Laboratory of Deep Oil and Gas, China University of Petroleum (East China),* 66 *Changjiang West Road, Huangdao District, Qingdao* 266580*, China*

[7] *Innovation Academy for Earth Science, Chinese Academy of Sciences,* 19 *Beitucheng Western Road, Chaoyang District, Beijing* 100029*, China*

Accepted 2020 February 28. Received 2020 February 21; in original form 2019 December 18

SUMMARY

The Lord–Shulman thermoelasticity theory combined with Biot equations of poroelasticity, describes wave dissipation due to fluid and heat flow. This theory avoids an unphysical behaviour of the thermoelastic waves present in the classical theory based on a parabolic heat equation, that is infinite velocity. A plane-wave analysis predicts four propagation modes: the classical *P* and *S* waves and two slow waves, namely, the Biot and thermal modes. We obtain the frequency-domain Green's function in homogeneous media as the displacements-temperature solution of the thermo-poroelasticity equations. The numerical examples validate the presence of the wave modes predicted by the plane-wave analysis. The *S* wave is not affected by heat diffusion, whereas the *P* wave shows an anelastic behaviour, and the slow modes present a diffusive behaviour depending on the viscosity, frequency and thermoelasticity properties. In heterogeneous media, the *P* wave undergoes mesoscopic attenuation through energy conversion to the slow modes. The Green's function is useful to study the physics in thermoelastic media and test numerical algorithms.

Key words: Heat flow; Seismic attenuation; Wave propagation.

1 INTRODUCTION

The study of the geomechanical properties of non-isothermal media is an important subject in many fields. The theory of thermoelasticity couples elastic deformations with the temperature field, based on the thermodynamics of irreversible processes (Biot 1956a; Deresiewicz 1957). The classical theory of poroelasticity has been established by Biot 1956b, 1962) for two-phase fluid-saturated porous media based on the Lagrange equations and Hamilton principle, which predicts the existence of a slow *P* wave (the Biot wave) besides the classical *P* and *S* waves. It has been verified experimentally (e.g. Plona 1980; Kelder & Smeulders 1997). The Biot wave is diffusive at low frequencies and has a lower velocity than that of the fast *P* wave at high frequencies.

Thermo-poroelasticity is an extension of the classical Biot theory, which combines the equation of heat conduction with the poroelasticity equations to describe the interaction between the displacement and temperature fields in porous media (Noda 1990; Nield & Bejan 2006). Bear *et al.* (1992) and Sharma (2008) developed mathematical models for wave propagation. The theory, if applied to heterogeneous media, also describes the important mechanism of wave-induced mesoscopic attenuation due to the presence of the elastic and thermal slow modes, which behave wave-like at high frequencies (Carcione *et al*. 2019, 2020). The thermal mode is diffusive for low values of the thermal conductivity and becomes wave-like for high values of this property. Compared to the uncoupled case (isothermal case), the fast *P* wave propagates at higher velocities and the *S* wave is not affected by the thermal flow. The theory is relevant in geophysical and geothermal exploration (Treitel 1959; Armstrong 1984; Cermak *et al.* 1990; Fu 2012, 2017; Jacquey *et al.* 2015; Poletto *et al.* 2018), and earthquake seismology (e.g. Boschi 1973; Simmons *et al.* 2010; Ritsema *et al.* 2011). In this work, we obtain the Green's function of thermo-poroelasticity, based on the Lord–Shulman theory.

The governing equation of thermoelasticity based on the parabolic-type equation of heat conduction has unphysical solutions such as discontinuities and infinite velocities as a function of frequency. As shown by Carcione *et al.* (2018), the heat equation can be generalized in analogy with the Maxwell model of viscoelasticity and the unphysical behaviour can be avoided by introducing relaxation terms into the heat equation, usually termed the Lord–Shulman model with a relaxation time (Lord & Shulman 1967; Green & Lindsay 1972; Eslami *et al.* 2013). Based on the Lord–Shulman thermoelasticity equations, Rudgers (1990) analyzed the physics and Carcione et al. (2018, 2019) generalized this theory to the poroelastic case and provided further insight into the physics by numerical simulations. A plane-wave analysis of the thermo-poroelasticity equations predicts the presence of a slow thermal wave (T wave) besides the classical P and S waves and Biot slow P wave. The presence of a slow T mode has been verified experimentally in solid helium and NaF crystals (e.g. Ackerman *et al.* 1966; Jackson *et al.* 1970; McNelly *et al.* 1970).

The Green's function plays an important role in many applications (e.g. Norris 1994; Fu & Bouchon 2004; Yang *et al.* 2007; Hu *et al.* 2009; Yu & Fu 2013; Wei & Fu 2019). There are many works, concerning classical thermoelasticity (e.g. Nowacki 1975; Kupradze *et al.* 1976; Tosaka 1985; Tosaka & Suh 1991), including Scarpetta *et al.* (2014) who obtained the Green's function for double-porosity media. Regarding the extended theory (hyperbolic heat equation), Wang *et al.* (2019) formulated a second-order tensor Green's function for the Lord–Shulman thermoelasticity equations.

In this work, we obtain the Green's function for the Lord–Shulman thermo-poroelasticity equations by means of elementary functions (Scarpetta 1990). First, we follow Carcione *et al.* (2019) and perform a plane-wave analysis to obtain the velocity and attenuation as a function of frequency. Then, we formulate the frequency-domain Green's function and, finally, wavefield snapshots are computed to further illustrate the physics.

2 THEORY OF THERMO-POROELASTICITY

The classical theory of thermo-poroelasticity is based on a parabolic equation of heat conduction, leading to infinite phase velocities. The modified equations with a relaxation term (Carcione *et al.* 2019) are briefly introduced in this section, which are the basis to develop the frequency-domain Green's function for wave propagation in non-isothermal porous media.

2.1 Equations of modified thermo-poroelasticity

The constitutive relations of thermo-poroelasticity for the stress components of the frame σ_{ij} and pore-fluid pressure p_f are (Carcione *et al.* 2019)

$$\begin{cases} \sigma_{ij} = \lambda\delta_{ij}u_{k,k} + \mu\left(u_{i,j} + u_{j,i}\right) + \alpha M\delta_{ij}\left(\alpha u_{k,k} + w_{k,k}\right) - \beta\delta_{ij}T \\ -p_f = M\left(\alpha u_{i,i} + w_{i,i}\right) - \dfrac{\beta_f}{\phi}T \end{cases}, \tag{1}$$

where λ and μ are the Lamé constants of the drained matrix, δ_{ij} is the Kronecker-delta, ϕ is the porosity, T is the increment of temperature over a reference T_0, u_i are the displacement components in the solid phase, U_i are the displacement components of the fluid phase,

$$\begin{cases} \alpha = 1 - \dfrac{K_m}{K_s}, \quad K_m = \lambda + \dfrac{2}{3}\mu \\ M = \dfrac{K_s}{1 - \phi - \dfrac{K_m}{K_s} + \phi\dfrac{K_s}{K_f}} \\ w_i = \phi\left(U_i - u_i\right), \beta = \beta_s + \alpha\beta_f \end{cases}, \tag{2}$$

where K_s and K_f are the solid and fluid bulk moduli, respectively, and β_s and β_f are the coefficients of thermal stress for the solid and fluid phases, respectively.

The dynamical equations are (Carcione *et al.* 2019)

$$\begin{cases} \sigma_{ij,j} = \rho\ddot{u}_i + \rho_f\ddot{w}_i \\ \left(-p_f\right)_{,i} = \rho_f\ddot{u}_i + q\ddot{w}_i + r\dot{w}_i \\ \gamma T_{,ii} = \rho C_e\left(\dot{T} + \tau_0\ddot{T}\right) + \beta T_0\left[\left(\dot{u}_{i,i} + \dot{w}_{i,i}\right) + \tau_0\left(\ddot{u}_{i,i} + \ddot{w}_{i,i}\right)\right] \end{cases}, \tag{3}$$

where γ is the coefficient of heat conduction, C_e is the specific heat capacity, $q = \tau\rho_f/\phi$, with τ the tortuosity and τ_0 is the relaxation time. The quantity $\rho = (1-\phi)\rho_s + \phi\rho_f$ is the composite density with ρ_s and ρ_f the solid and fluid densities, respectively. The Darcy law defines the movement of viscous fluids of viscosity η in the frame of permeability χ, and $r = \eta/\chi$.

Thus, the non-isothermal wave equations for isotropic porous media saturated with a viscous fluid are

$$\begin{cases} \rho\ddot{u}_i + \rho_f\ddot{w}_i = \left(\lambda + \mu + \alpha^2 M\right)u_{j,ij} + \mu u_{i,jj} + \alpha M w_{j,ij} - \beta T_{,i} \\ \rho_f\ddot{u}_i + q\ddot{w}_i + r\dot{w}_i = M\left(\alpha u_{j,ij} + w_{j,ij}\right) - \dfrac{\beta_f}{\phi}T_{,i} \\ \gamma T_{,ii} = \rho C_e\left(\dot{T} + \tau_0\ddot{T}\right) + \beta T_0\left[\dot{u}_{i,i} + \dot{w}_{i,i} + \tau_0\left(\ddot{u}_{i,i} + \ddot{w}_{i,i}\right)\right] \end{cases}. \tag{4}$$

2.2 Plane-wave analysis

To examine the characteristics of wave propagation in thermo-poroelastic media, we consider the following plane-wave expressions

$$\begin{cases} u_i = As_i e^{\mathrm{i}\omega\left(t-\frac{l_j}{v_c}x_j\right)} \\ w_i = Bd_i e^{\mathrm{i}\omega\left(t-\frac{l_j}{v_c}x_j\right)} \\ T = Ce^{\mathrm{i}\omega\left(t-\frac{l_j}{v_c}x_j\right)} \end{cases}, \tag{5}$$

where s_i and d_i are the polarizations for the motions of the solid and fluid particles, respectively, A, B and C are amplitude constants, ω is the angular frequency, t is the time, v_c is the complex velocity, l_j denotes the propagation directions, x_j are the position components and $\mathrm{i} = \sqrt{-1}$.

Substituting eq. (5) into (4) yields a system of algebraic equations,

$$\begin{cases} (\lambda+\mu+\alpha^2 M)\left(\frac{\omega}{v_c}\right)^2 As_jl_jl_i + \alpha M\left(\frac{\omega}{v_c}\right)^2 Bd_jl_jl_i + \mu\left(\frac{\omega}{v_c}\right)^2 As_i - \rho\omega^2 As_i - \rho_f\omega^2 Bd_i - \mathrm{i}\frac{\omega}{v_c}\beta C\, l_i = 0 \\ M\left(\alpha\left(\frac{\omega}{v_c}\right)^2 As_jl_jl_i + \left(\frac{\omega}{v_c}\right)^2 Bd_jl_jl_i\right) - \rho_f A\omega^2 s_i - qB\omega^2 d_i + r\mathrm{i}\omega Bd_i - \mathrm{i}\frac{\beta_f}{\phi}\frac{\omega}{v_c}C\, l_i = 0 \\ \rho C_e\left(\mathrm{i}\omega C - \tau_0\omega^2 C\right) + \beta T_0\left[\frac{\omega}{v_c}\omega As_il_i + \frac{\omega}{v_c}\omega Bd_il_i + \tau_0\left(\mathrm{i}\frac{\omega}{v_c}\omega^2 As_il_i + \mathrm{i}\frac{\omega}{v_c}\omega^2 Bd_il_i\right)\right] + \gamma\left(\frac{\omega}{v_c}\right)^2 C = 0 \end{cases}. \tag{6}$$

For S waves, $s_i\ l_i = d_i\ \ l_i = 0$, and the direction of propagation is perpendicular to the direction of displacement, and

$$v_c^S = \sqrt{\frac{\mu}{\rho - \frac{\rho_f^2}{q-\mathrm{i}\frac{r}{\omega}}}}. \tag{7}$$

We see that S-wave propagation is independent of the thermal properties in isotropic thermo-poroelastic media.

For P waves, $s_i\ l_i = d_i\ \ l_i = 1$, and the direction of propagation is parallel to the direction of displacement. The resulting dispersion relation can be solved by a cubic equation in v_c^2 as

$$a\left(v_c^2\right)^3 + b\left(v_c^2\right)^2 + cv_c^2 + d = 0, \tag{8}$$

where

$$\begin{cases} a = \rho C_e\phi N(\omega L - \mathrm{i}r\rho) \\ b = \mathrm{i}\phi rK - \omega(r\phi(\gamma\rho + \tau_0 K) + \phi\rho C_e H + T_0\beta J) - \mathrm{i}\omega^2(\phi(\gamma L + \rho C_e H\tau_0) + T_0\beta J\tau_0) \\ c = \omega(\phi(\rho C_e ME + r\gamma F) + T_0\beta G) + \mathrm{i}\omega^2(\phi(\gamma H + \rho C_e ME\tau_0) + T_0\beta G\tau_0) \\ d = -\mathrm{i}\omega^2\gamma\phi ME \end{cases}, \tag{9}$$

with

$$\begin{cases} E = \lambda + 2\mu,\ F = E + \alpha^2 M,\ G = E\beta_f + M(\alpha - 1)\left(\alpha\beta_f - \phi\beta\right) \\ H = qF + \rho M - 2\alpha M\rho_f,\ J = \beta_f\left(\rho - \rho_f\right) + \phi\beta\left(q - \rho_f\right),\ K = \rho C_e F + T_0\beta^2 \\ L = q\rho - {\rho_f}^2,\ N = 1 + i\omega\tau_0 \end{cases}. \tag{10}$$

We see that the fast P waves are dissipative due to the coupling with the Biot and heat flow.

3 GREEN'S FUNCTION FOR THERMO-POROELASTICITY

We formulate the frequency-domain Green's function for thermo-poroelasticity. We first apply a Fourier transform to eq. (4),

$$\bar{u}\left(\vec{x},\omega\right) = \int_{-\infty}^{\infty} u\left(\vec{x},t\right)\mathrm{e}^{-\mathrm{i}\omega t}\mathrm{d}t, \tag{11}$$

leading to the following differential equations in the frequency domain (omitting the hat for convenience):

$$\begin{cases} a_1 u_{j,ij} + \mu u_{i,jj} + \rho\omega^2 u_i + \alpha M w_{j,ij} + \rho_f\omega^2 w_i - \beta\ T_{,i} = 0 \\ M\left(\alpha u_{j,ij} + w_{j,ij}\right) + \rho_f\omega^2 u_i + a_2 w_i - \frac{\beta_f}{\phi}\ T_{,i} = 0 \\ \gamma T_{,ii} + \rho C_e a_3 T + \beta T_0 a_3\ (u_{i,i} + w_{i,i}) = 0 \end{cases}, \tag{12}$$

where $a_1 = \lambda + \mu + \alpha^2 M$, $a_2 = q\omega^2 - \mathrm{i}\omega r$ and $a_3 = \tau_0\ \omega^2 - \mathrm{i}\omega$.

To derive the Green's function for eq. (12), we introduce the following matrix differential operator based on eq. (12):

$$\mathrm{A}(\nabla)=\begin{bmatrix} a_1\nabla\mathrm{div}+\mu\Delta+\rho\omega^2 & \alpha M\nabla\mathrm{div}+\rho_f\omega^2 & -\beta\mathrm{div} \\ \alpha M\nabla\mathrm{div}+\rho_f\omega^2 & M\nabla\mathrm{div}+a_2 & -\dfrac{\beta_f}{\phi}\mathrm{div} \\ \beta T_0 a_3\nabla & \beta T_0 a_3\nabla & \gamma\Delta+\rho C_e a_3 \end{bmatrix}, \tag{13}$$

where div is the divergence symbol, and consider the system of non-homogeneous equations:

$$\begin{bmatrix} a_1\nabla\mathrm{div}+\mu\Delta+\rho\omega^2 & \alpha M\nabla\mathrm{div}+\rho_f\omega^2 & \beta T_0 a_3\nabla \\ \alpha M\nabla\mathrm{div}+\rho_f\omega^2 & M\nabla\mathrm{div}+a_2 & \beta T_0 a_3\nabla \\ -\beta\mathrm{div} & -\dfrac{\beta_f}{\phi}\mathrm{div} & \gamma\Delta+\rho C_e a_3 \end{bmatrix}\begin{bmatrix}\vec{u}\\ \vec{w}\\ T\end{bmatrix}=\begin{bmatrix}\vec{f}_1\\ \vec{f}_2\\ f_3\end{bmatrix}, \tag{14}$$

or

$$\mathrm{A}^{\mathrm{T}}(\nabla)\ \vec{\alpha}=\vec{\mathrm{b}}, \tag{15}$$

where $\mathrm{A}^{\mathrm{T}}(\nabla)$ is the transpose of matrix differential operator $\mathrm{A}(\nabla)$,

$$\mathrm{A}^{\mathrm{T}}(\nabla)=\begin{bmatrix} a_1\nabla\mathrm{div}+\mu\Delta+\rho\omega^2 & \alpha M\nabla\mathrm{div}+\rho_f\omega^2 & \beta T_0 a_3\nabla \\ \alpha M\nabla\mathrm{div}+\rho_f\omega^2 & M\nabla\mathrm{div}+a_2 & \beta T_0 a_3\nabla \\ -\beta\mathrm{div} & -\frac{\beta_f}{\phi}\mathrm{div} & \gamma\Delta+\rho C_e a_3 \end{bmatrix},$$

$$\vec{\alpha}=\begin{bmatrix}\vec{u}\\ \vec{w}\\ T\end{bmatrix},\ \text{and}\ \vec{b}=\begin{bmatrix}\vec{f}_1\\ \vec{f}_2\\ f_3\end{bmatrix},$$

$\vec{f}_1$ and $\vec{f}_2$ are two-component vector functions and f_3 is a scalar function.

Applying the divergence operator to the first and second terms of eq. (14), we obtain

$$\mathrm{B}(\Delta)\ \vec{\beta}=\vec{c}, \tag{16}$$

where

$$\mathrm{B}\ (\Delta)=\begin{bmatrix} a_0\Delta+\rho\omega^2 & \alpha M\Delta+\rho_f\omega^2 & \beta T_0 a_3\Delta \\ \alpha M\Delta+\rho_f\omega^2 & M\Delta+a_2 & \beta T_0 a_3\Delta \\ -\beta & -\frac{\beta_f}{\phi} & \gamma\Delta+\rho C_e a_3 \end{bmatrix},\ \text{with}\ a_0=a_1+\mu,$$

$$\vec{\beta}=\begin{bmatrix}\mathrm{div}\vec{u}\\ \mathrm{div}\vec{w}\\ T\end{bmatrix},\ \text{and}\ \vec{c}=\begin{bmatrix}\mathrm{div}\vec{f}_1\\ \mathrm{div}\vec{f}_2\\ f_3\end{bmatrix}.$$

By introducing the operator

$$\Lambda_1\ (\Delta)=\frac{1}{\gamma M a_0}\ \mathrm{detB}\ (\Delta)=\prod_{i=1}^{3}\left(\Delta+\lambda_i^2\right),$$

the following equation

$$\Lambda_1(\Delta)\ \vec{\beta}=\vec{g} \tag{17}$$

can be obtained from eq. (16), where

$$g_j=\frac{1}{\gamma M a_0}\sum_{i=1}^{3}B_{ij}^{*}(\Delta)\,c_i, \tag{18}$$

with $B_{ij}^{*}(\Delta)$ the cofactor of the element $B_{ij}(\Delta)$ of matrix $\mathrm{B}(\Delta)$.

From the first and second terms of eq. (14), we have

$$\begin{cases}\left(\mu\Delta+\rho\omega^2\right)\vec{u}+\rho_f\omega^2\ \vec{w}=\vec{f}_1-a_1\nabla\beta_1-\alpha M\nabla\beta_2-\beta T_0 a_3\nabla\beta_3\\ \rho_f\omega^2\vec{u}+a_2\ \vec{w}=\vec{f}_2-M\left(\alpha\nabla\beta_1+\nabla\beta_2\right)-\beta T_0 a_3\nabla\beta_3\end{cases}. \tag{19}$$

Then, we apply the divergence operator $\Lambda_1(\Delta)$ to eq. (19) to yield

$$\mathrm{C}(\Delta)\ \vec{\gamma} = \vec{d}\,, \tag{20}$$

where

$$\mathrm{C}(\Delta) = \begin{bmatrix} \mu\Delta + \rho\omega^2 & \rho_f\omega^2 \\ \rho_f\omega^2 & a_2 \end{bmatrix},$$

$$\vec{\gamma} = \begin{bmatrix} \Lambda_1(\Delta)\vec{u} \\ \Lambda_1(\Delta)\vec{w} \end{bmatrix}, \text{ and } \vec{d} = \begin{bmatrix} \Lambda_1\vec{f}_1 - a_1\nabla g_1 - \alpha M\nabla g_2 - \beta T_0 a_3\nabla g_3 \\ \Lambda_1\vec{f}_2 - M(\alpha\nabla g_1 + \nabla g_2) - \beta T_0 a_3\nabla g_3 \end{bmatrix}.$$

By introducing the operator

$$\Lambda_2(\Delta) = \frac{\Lambda_1(\Delta)}{\mu a_2}\det\mathrm{C}\ (\Delta) = \Lambda_1\ (\Delta)\left(\Delta + \lambda_4^2\right), \tag{21}$$

where

$$\lambda_4^2 = \frac{\rho\omega^2}{\mu} - \frac{{\rho_f}^2\omega^4}{a_2\mu},$$

the following equation

$$\frac{1}{\mu a_2}\det\mathrm{C}(\Delta)\begin{bmatrix} \Lambda_1(\Delta)\vec{u} \\ \Lambda_1(\Delta)\vec{w} \end{bmatrix} = \begin{bmatrix} \Lambda_2(\Delta) & 0 \\ 0 & \Lambda_2(\Delta) \end{bmatrix}\begin{bmatrix} \vec{u} \\ \vec{w} \end{bmatrix} = \begin{bmatrix} h_1 \\ h_2 \end{bmatrix}, \tag{22}$$

can be obtained from eqs (17), (20) and (21), where

$$h_j = \frac{1}{\mu a_2}\sum_{i=1}^{2} C_{ij}^*(\Delta)\, d_i, \tag{23}$$

with $C_{ij}^*(\Delta)$ being the cofactor of the element $C_{ij}(\Delta)$ of matrix $\mathrm{C}(\Delta)$.

On the basis of eqs (17) and (22), we have

$$\Lambda(\Delta)\ \vec{\alpha} = \vec{m}\,, \tag{24}$$

where

$$\Lambda(\Delta)\vec{\alpha} = \begin{bmatrix} \Lambda_2(\Delta) & 0 & 0 \\ 0 & \Lambda_2(\Delta) & 0 \\ 0 & 0 & \Lambda_1(\Delta) \end{bmatrix}\begin{bmatrix} \vec{u} \\ \vec{w} \\ T \end{bmatrix}, \text{ and } \vec{m} = \begin{bmatrix} h_1 \\ h_2 \\ g_3 \end{bmatrix}.$$

From eqs (18) and (23), $\vec{m}$ can be expanded as follows:

$$\vec{m} = \begin{bmatrix} \dfrac{1}{\mu a_2}\displaystyle\sum_{i=1}^{2} C_{i1}^*(\Delta)\, d_i \\ \dfrac{1}{\mu a_2}\displaystyle\sum_{i=1}^{2} C_{i2}^*(\Delta)\, d_i \\ \dfrac{1}{\gamma M a_0}\displaystyle\sum_{i=1}^{3} B_{i3}^*(\Delta)\, c_i \end{bmatrix}. \tag{25}$$

We separate eq. (25) into the following operator product form

$$\vec{m} = \begin{bmatrix} \dfrac{C_{11}^*}{\mu a_2} & \dfrac{C_{21}^*}{\mu a_2} & 0 \\ \dfrac{C_{12}^*}{\mu a_2} & \dfrac{C_{22}^*}{\mu a_2} & 0 \\ 0 & 0 & \dfrac{I}{\gamma M a_0} \end{bmatrix}\begin{bmatrix} \Lambda_1\vec{f}_1 - a_1\nabla g_1 - \alpha M\nabla g_2 - \beta T_0 a_3\nabla g_3 \\ \Lambda_1\vec{f}_2 - M(\alpha\nabla g_1 + \nabla g_2) - \beta T_0 a_3\nabla g_3 \\ B_{13}^*\mathrm{div}\vec{f}_1 + B_{23}^*\mathrm{div}\vec{f}_2 + B_{33}^* f_3 \end{bmatrix}. \tag{26}$$

Using to eq. (18), eq. (26) can be expressed as

Table 1. Material properties.

Grain bulk modulus, $\boldsymbol{K_s}$	35 GPa
Density, $\boldsymbol{\rho_s}$	2650 kg m^{-3}
Frame bulk modulus, $\boldsymbol{K_m}$	1.7 GPa
Shear modulus, $\boldsymbol{\mu_m}$	1.885 GPa
Porosity, ϕ	0.3
Permeability, $\boldsymbol{\chi}$	1 darcy
Tortuosity, $\boldsymbol{\tau}$	2
Water density, $\boldsymbol{\rho_f}$	1000 kg m^{-3}
Viscosity, $\boldsymbol{\eta}$	0.001 Pa · s
Bulk modulus, $\boldsymbol{K_f}$	2.4 GPa
Thermoelasticity coefficient, $\boldsymbol{\beta_f}$	40 000 kg (m · s^2 · deg K)$^{-1}$
Bulk specific heat capacity, $\boldsymbol{C_e}$	0.38 m^2 (s^2 · deg K)$^{-1}$
Thermoelasticity coefficient, $\boldsymbol{\beta}$	120 000 kg (m · s^2 · deg K)$^{-1}$
Absolute temperature, $\boldsymbol{T_0}$	300 °K

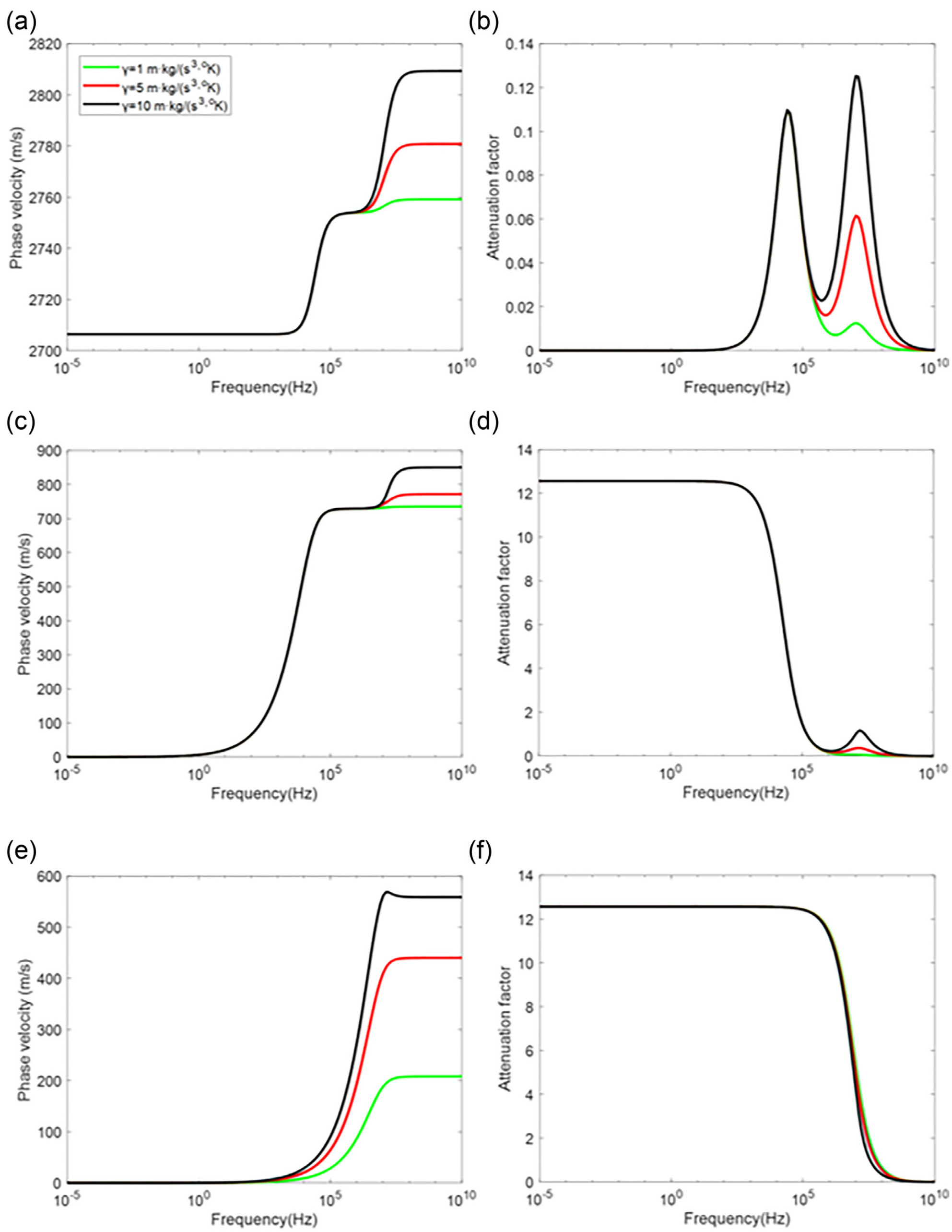

Figure 1. Phase velocity and attenuation factor of the *P* wave (a and b), slow *P* wave (c and d) and *T* wave (e and f) as a function of frequency for different thermal conductivities.

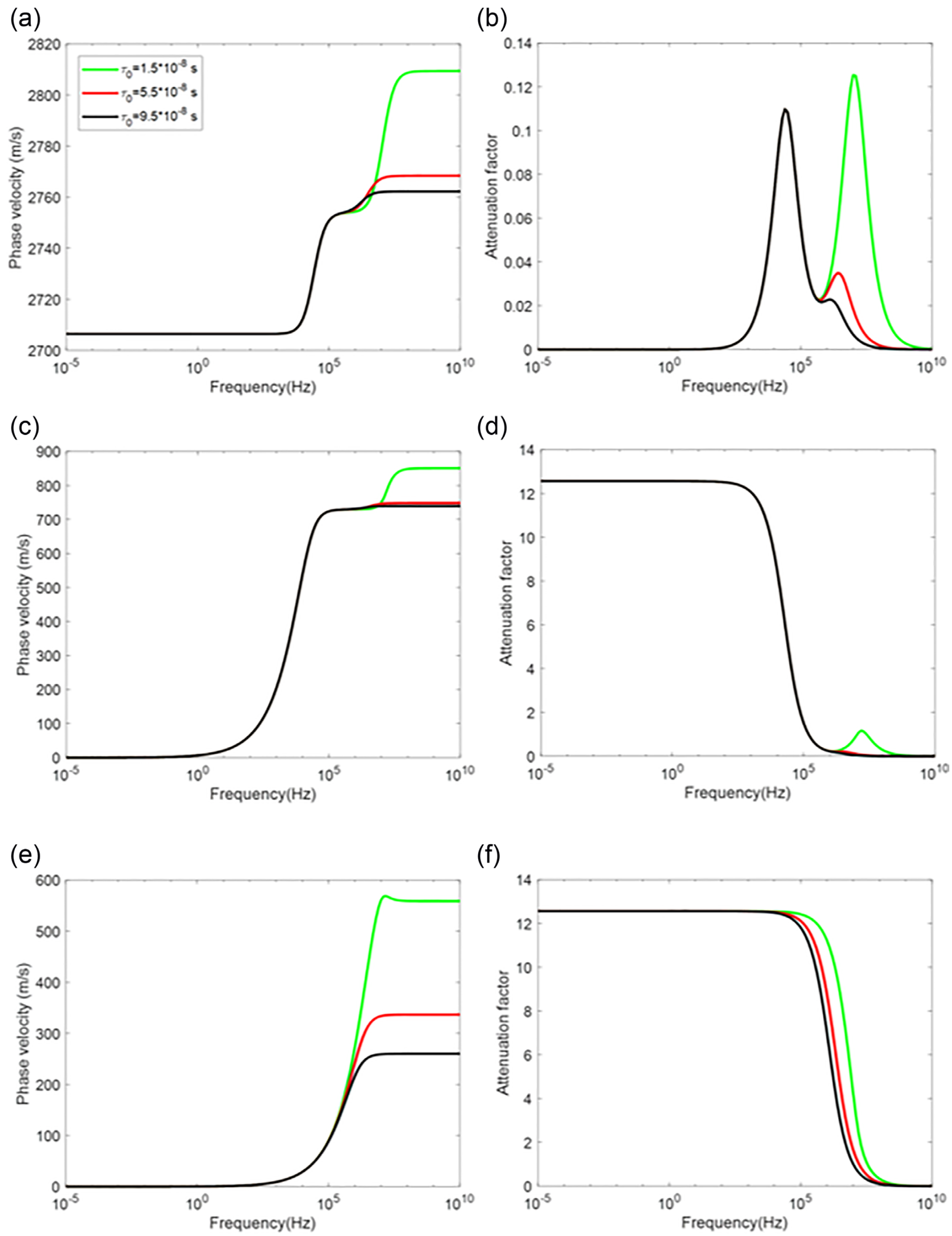

Figure 2. Phase velocity and attenuation factor of the P wave (a and b), slow P wave (c and d) and T wave (e and f) as a function of frequency for different relaxation times.

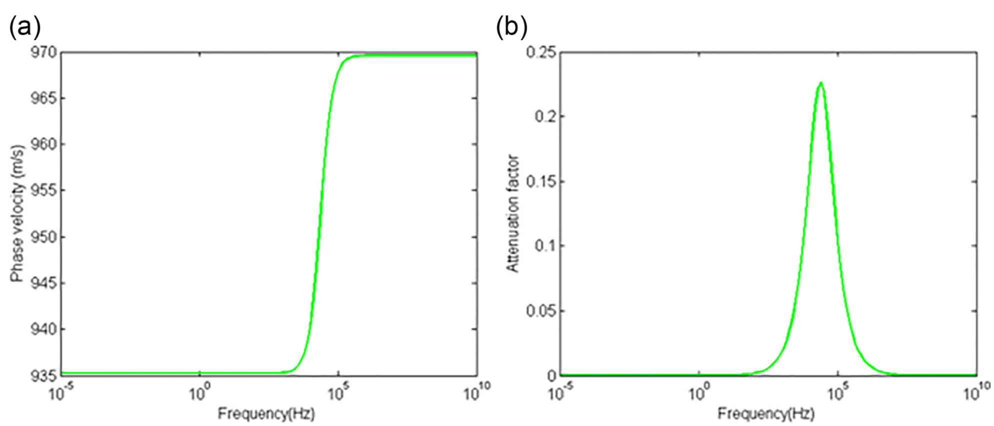

Figure 3. Phase velocity and attenuation factor of the S wave (a and b) as a function of frequency.

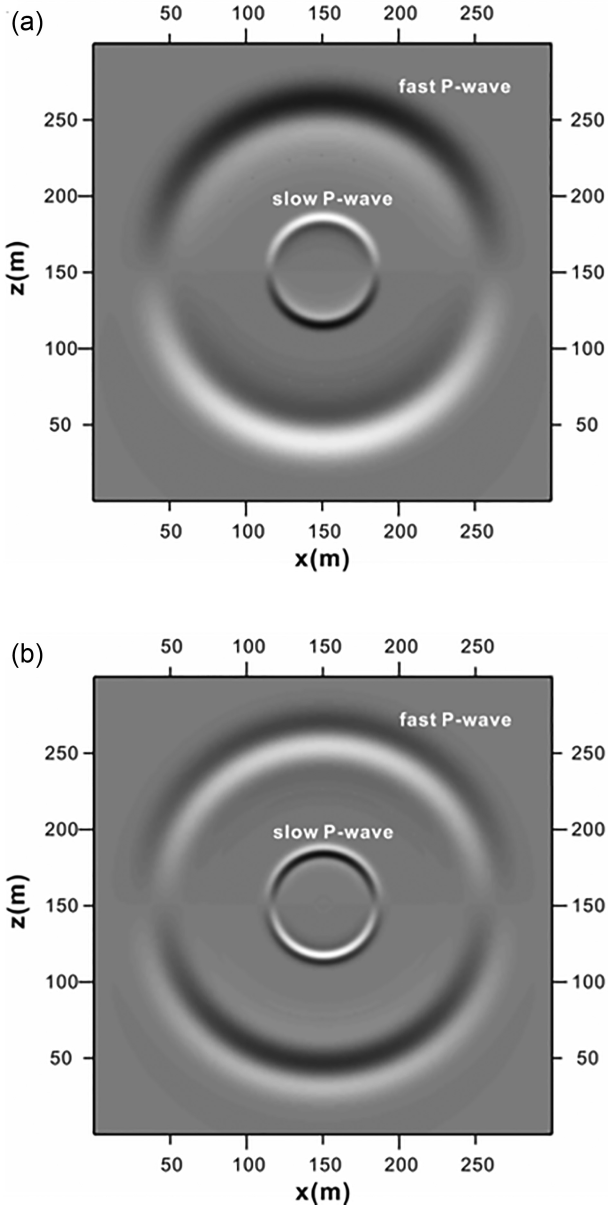

Figure 4. (a) Particle-velocity u_z at 50 ms with $\eta = 0$ due to a heat source and (b) temperature T at 50 ms with $\eta = 0$ due to a vertical elastic force for $\gamma = 5\ \mathrm{m} \cdot \mathrm{kg}\,(\mathrm{s}^3 \cdot \mathrm{deg\,K})^{-1}$ with $\tau_0 = 1.5 \times 10^{-8}$ s.

$$\vec{m} = \begin{bmatrix} \dfrac{C_{11}^*}{\mu a_2} & \dfrac{C_{21}^*}{\mu a_2} & 0 \\ \dfrac{C_{12}^*}{\mu a_2} & \dfrac{C_{22}^*}{\mu a_2} & 0 \\ 0 & 0 & \dfrac{I}{\gamma M a_0} \end{bmatrix} \begin{bmatrix} \Lambda_1 \vec{f}_1 - \dfrac{1}{\gamma M a_0}\left(a_1 \nabla \sum_{i=1}^{3} B_{i1}^* c_i + \alpha M \nabla \sum_{i=1}^{3} B_{i2}^* c_i + \beta T_0 a_3 \nabla \sum_{i=1}^{3} B_{i3}^* c_i\right) \\ \Lambda_1 \vec{f}_2 - \dfrac{1}{\gamma M a_0}\left(M\left(\alpha \nabla \sum_{i=1}^{3} B_{i1}^* c_i + \nabla \sum_{i=1}^{3} B_{i2}^* c_i\right) + \beta T_0 a_3 \nabla \sum_{i=1}^{3} B_{i3}^* c_i\right) \\ B_{13}^* \operatorname{div} \vec{f}_1 + B_{23}^* \operatorname{div} \vec{f}_2 + B_{33}^* f_3 \end{bmatrix}. \tag{27}$$

By introducing the following notation:

$$n_{i1}\,(\Delta) = -\frac{1}{\gamma M a_0}\left(a_1 B_{i1}^*(\Delta) + \alpha M B_{i2}^*(\Delta) + \beta T_0 a_3 B_{i3}^*(\Delta)\right),$$

$$n_{i2}\,(\Delta) = -\frac{1}{\gamma M a_0}\left(M\left(\alpha B_{i1}^*(\Delta) + B_{i2}^*(\Delta)\right) + \beta T_0 a_3 B_{i3}^*(\Delta)\right) \text{ and } n_{i3}\,(\Delta) = \frac{1}{\gamma M a_0}\, B_{i3}^*(\Delta),$$

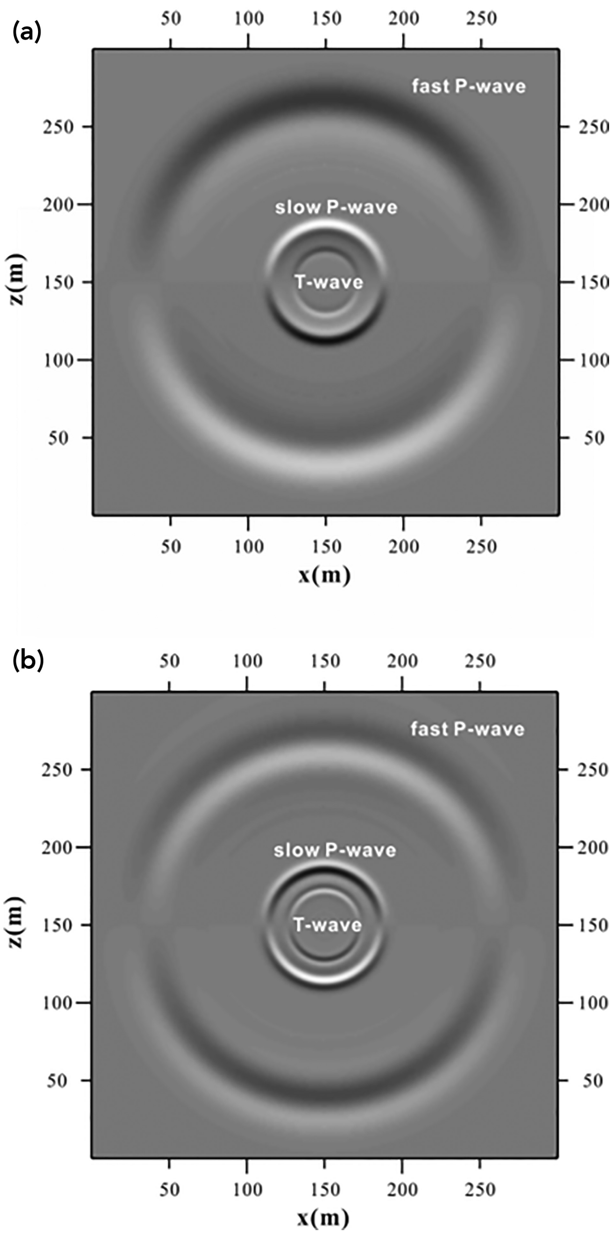

Figure 5. (a) Particle-velocity u_z at 50 ms with $\eta = 0$ due to a heat source and (b) temperature T at 50 ms with $\eta = 0$ due to a vertical elastic force for $\gamma = 4.5 \times 10^6$ m kg $(\mathrm{s}^3 \cdot \deg \mathrm{K})^{-1}$ with $\tau_0 = 1.5 \times 10^{-2}$ s.

we have

$$\vec{m} = \begin{bmatrix} \frac{C_{11}^*}{\mu a_2} & \frac{C_{21}^*}{\mu a_2} & 0 \\ \frac{C_{12}^*}{\mu a_2} & \frac{C_{22}^*}{\mu a_2} & 0 \\ 0 & 0 & I \end{bmatrix} \begin{bmatrix} \Lambda_1 + n_{11}\nabla\mathrm{div} & n_{21}\nabla\mathrm{div} & n_{31}\nabla \\ n_{12}\nabla\mathrm{div} & \Lambda_1 + n_{22}\nabla\mathrm{div} & n_{32}\nabla \\ n_{13}\mathrm{div} & n_{23}\mathrm{div} & n_{33} \end{bmatrix} \begin{bmatrix} \vec{f}_1 \\ \vec{f}_2 \\ f_3 \end{bmatrix}, \tag{28}$$

By combining eqs (15) and (28), we obtain the following operator,

$$\mathrm{L}^{\mathrm{T}} = \begin{bmatrix} \frac{C_{11}^*}{\mu a_2} & \frac{C_{21}^*}{\mu a_2} & 0 \\ \frac{C_{12}^*}{\mu a_2} & \frac{C_{22}^*}{\mu a_2} & 0 \\ 0 & 0 & I \end{bmatrix} \begin{bmatrix} \Lambda_1 + n_{11}\nabla\mathrm{div} & n_{21}\nabla\mathrm{div} & n_{31}\nabla \\ n_{12}\nabla\mathrm{div} & \Lambda_1 + n_{22}\nabla\mathrm{div} & n_{32}\nabla \\ n_{13}\mathrm{div} & n_{23}\mathrm{div} & n_{33} \end{bmatrix}, \tag{29}$$

because

$$\mathrm{L}^{\mathrm{T}}\vec{b} = \vec{m},$$

$$\Lambda\,\vec{\alpha} = \mathrm{L}^{\mathrm{T}}\,\mathrm{A}^{\mathrm{T}}\vec{\alpha},$$

thus

$$\mathrm{AL} = \Lambda.$$

We also introduce the matrix

$$\Phi = \begin{bmatrix} \Phi_2 & 0 & 0 \\ 0 & \Phi_2 & 0 \\ 0 & 0 & \Phi_1 \end{bmatrix}, \tag{30}$$

where $\Phi_1 = \sum_{j=1}^{3} \eta_{1j}\gamma^{(j)}(\vec{x})$ and $\Phi_2 = \sum_{j=1}^{4} \eta_{2j}\gamma^{(j)}(\vec{x})$, with

$$\begin{cases} \gamma^{(j)}\left(\vec{x}\right) = \frac{i}{4}\, H_0^{(1)}\left(\lambda_j \left|\vec{x}\right|\right), \\ \eta_{1j} = \prod_{i=1, i\neq j}^{3} \left(\lambda_i^2 - \lambda_j^2\right)^{-1}, \quad (j = 1, 2, 3;\ k = 1, 2, 3, 4) \\ \eta_{2k} = \prod_{i=1, i\neq k}^{4} \left(\lambda_i^2 - \lambda_k^2\right)^{-1}, \end{cases}$$

to constitute the Green's function of the Helmholtz equation $(\Delta + \lambda_j^2)\gamma^{(j)}\,(\vec{x}) = -\delta(\vec{x})$. According to Scarpetta *et al.* (2014) (Lemma 1), we have

$$\mathrm{AL}\Phi = \Lambda\Phi = \mathrm{I}.$$

Thus, the Green's function becomes

$$\mathrm{V} = \mathrm{L}\Phi, \tag{31}$$

where

$$\mathrm{L} = \begin{bmatrix} \Lambda_1 + n_{11}\nabla\mathrm{div} & n_{12}\nabla\mathrm{div} & n_{13}\nabla \\ n_{21}\nabla\mathrm{div} & \Lambda_1 + n_{22}\nabla\mathrm{div} & n_{23}\nabla \\ n_{31}\mathrm{div} & n_{32}\mathrm{div} & n_{33} \end{bmatrix} \begin{bmatrix} \frac{C_{11}^*}{\mu a_2} & \frac{C_{12}^*}{\mu a_2} & 0 \\ \frac{C_{21}^*}{\mu a_2} & \frac{C_{22}^*}{\mu a_2} & 0 \\ 0 & 0 & I \end{bmatrix},$$

leading to

$$\mathrm{V} = \begin{bmatrix} (\Lambda_1 + n_{11}\nabla\mathrm{div})\,\frac{C_{11}^*}{\mu a_2}\Phi_2 + n_{12}\nabla\mathrm{div}\frac{C_{21}^*}{\mu a_2}\Phi_2 & (\Lambda_1 + n_{11}\nabla\mathrm{div})\,\frac{C_{12}^*}{\mu a_2}\Phi_2 + n_{12}\nabla\mathrm{div}\frac{C_{22}^*}{\mu a_2}\Phi_2 & n_{13}\nabla\Phi_1 \\ n_{21}\nabla\mathrm{div}\frac{C_{11}^*}{\mu a_2}\Phi_2 + (\Lambda_1 + n_{22}\nabla\mathrm{div})\,\frac{C_{21}^*}{\mu a_2}\Phi_2 & n_{21}\nabla\mathrm{div}\frac{C_{12}^*}{\mu a_2}\Phi_2 + (\Lambda_1 + n_{22}\nabla\mathrm{div})\,\frac{C_{22}^*}{\mu a_2}\Phi_2 & n_{23}\nabla\Phi_1 \\ n_{31}\mathrm{div}\frac{C_{11}^*}{\mu a_2}\Phi_2 + n_{32}\mathrm{div}\frac{C_{21}^*}{\mu a_2}\Phi_2 & n_{31}\mathrm{div}\frac{C_{12}^*}{\mu a_2}\Phi_2 + n_{32}\mathrm{div}\frac{C_{22}^*}{\mu a_2}\Phi_2 & n_{33}\Phi_1 \end{bmatrix}. \tag{32}$$

4 NUMERICAL EXAMPLES

We consider the thermo-poroelastic model with material properties (Table 1) given by Carcione *et al.* (2019), although the value C_e is actually low for rocks. A plane-wave analysis and a simulation for wavefield snapshots are conducted in this section to illustrate the dispersion and attenuation properties of thermo-poroelastic waves. Wave velocity and attenuation are calculated as a function of frequency for two sets of thermal properties: (1) $\tau_0 = 1.5 \times 10^{-8}$ s with $\gamma = 1$, 5 and 10 $\mathrm{m\cdot kg\,(s^3\cdot deg\,K)^{-1}}$ and (2) $\gamma = 10\ \mathrm{m\cdot kg\,(s^3\cdot deg\,K)^{-1}}$ with $\tau_0 = 1.5 \times 10^{-8}$, 5.5×10^{-8} and 9.5×10^{-8} s. The phase velocity $v_p = 1/[\mathrm{Re}(1/v_c)]$ and the attenuation factor $A_p = -4\pi v_p \mathrm{Im}(1/v_c)$ can be obtained from the complex velocity v_c as a function of frequency (see eqs 7 and 8).

Fig. 1 shows the phase velocity and attenuation of thermo-poroelastic waves as a function of frequency for the first set of thermal properties. We see that the thermo-poroelastic dispersion is of a dual-peak structure in both the phase velocity and quality factor. In general, the velocity dispersion with frequencies is relevant to intrinsic attenuation. The dual-peak feature of dispersion is strongly associated with classical Biot loss and heat diffusion. The wave-like *T* mode has characteristics similar to the Biot slow diffusive wave, since the poroelasticity and thermoelasticity have similar constitutive relations. Both the slow *P* and *T* waves are highly attenuated toward low frequencies. We note that the second peak in both the phase velocity and attenuation becomes strong with increasing thermal conductivities. In conclusion, the velocity and attenuation dispersions for *P*, slow *P* and *T* waves increase with increasing thermal conductivities.

Fig. 2 shows the phase velocity and attenuation with frequencies for P, slow P and T waves at different relaxation times. We see that the second peak in both the phase velocity and attenuation for all the modes is significantly affected by relaxation times, becoming weak with increasing relaxation times. Nevertheless, the wave-like T mode is prone to be observed in either high thermal conductivities or small relaxation times within the high-frequency band. Fig. 3 shows the phase velocity and attenuation as a function of frequency for S wave, obtained from eq. (7). We see that the S wave has only one attenuation peak due to the Biot loss, which is independent of heat diffusion. We have to stress that the physics of thermo-poroelastic dispersion is rather complex and could be addressed by incorporating laboratory measurements in the future.

Snapshots are calculated by the Green's function (eq. 32) for two sets of thermal properties (1) $\gamma = 5\,\mathrm{m\,kg\,(s^3 \cdot deg\,K)^{-1}}$ with $\tau_0 = 1.5 \times 10^{-8}$ s and (2) $\gamma = 4.5 \times 10^6\ \mathrm{m \cdot kg\,(s^3 \cdot deg\,K)}$ with $\tau_0 = 1.5 \times 10^{-2}$ s. The source, located at the center of the mesh, is a Ricker wavelet with the central frequency of 150 Hz. The wavefields generated by a heat source and a vertical elastic force at 50 ms with $\eta = 0$ are calculated for two sets of thermal properties, with the results shown in Figs 4 and 5, respectively. We observe that the T wave is diffuse and weak. As expected from Figs 1 and 2, it is hard to see the mode in Fig. 4 with small thermal conductivities, which, however, becomes obvious in Fig. 5 with large thermal conductivities. Different dilatational waves can be seen in Figs 4 and 5, where the heat source generates significant compressional waves, but there is no shear wave. The S wave can be generated by the vertical elastic force, but this mode is not present the temperature field.

5 CONCLUSIONS

We have derived the frequency-domain Green's function of the Lord–Shulman thermo-poroelasticity theory, where the displacement-temperature fields are obtained for isotropic porous media. Our numerical results clearly show the presence of a slow thermal P wave (the T wave) besides the classical *P and S* waves and the diffusive/wave-like Biot P mode. The S wave is not affected by the thermal effects, but the three P waves exhibit a lossy behaviour under certain conditions, which depends on the viscosity, frequency and thermoelastic constants. In the seismic frequency band, the T and Biot waves are highly attenuated and are coupled with the fast P wave inducing energy dissipation at high frequencies.

ACKNOWLEDGEMENTS

The authors are very grateful to the editor and two reviewers for their constructive reviews. The research was supported by the Major State Research Development Program of China (Grant no. 2016YFC0601101), and the PetroluemChina Project (Grant no. 2016A-4801).

REFERENCES

Ackerman, C.C., Bertman, B., Fairbank, H.A. & Guyer, R.A., 1966. Second sound in solid helium, *Phys. Rev. Lett.,* **16,** 789.

Armstrong, B.H., 1984. Models for thermoelastic attenuation of waves in heterogeneous solids, *Geophysics,* **49,** 1032–1040.

Bear, J., Sorek, S., Ben-Dor, G. & Mazor, G., 1992. Displacement waves in saturated thermoelastic porous media. I. Basic equations, *Fluid Dyn. Res.,* **9,** 155–164.

Biot, M.A., 1956a. Thermoelasticity and irreversible thermodynamics, *J. appl. Phys.,* **27,** 240–253.

Biot, M.A., 1956b. The theory of propagation of elastic waves in a fluid-saturated porous solid - I. Low-frequency range II. Higher frequency range, *J. acoust. Soc. Am.,* **28,** 168–191.

Biot, M.A., 1962. Mechanics of deformation and acoustic propagation in porous media, *J. appl. Phys.,* **33,** 1482–1498.

Boschi, E., 1973. A thermoviscoelastic model of the earthquake source mechanism, *J. geophys. Res.,* **78,** 7733–7737.

Carcione, J.M., Gei, D., Santos, J.E., Fu, L.-Y. & Ba, J., 2020. Canonical analytical solutions of wave-induced thermoelastic attenuation, *Geophys. J. Int.,* **221** (2), 835–842.

Carcione, J.M., Cavallini, F., Wang, E., Ba, J. & Fu, L.Y., 2019. Physics and simulation of wave propagation in linear thermo-poroelastic media, *J. geophys. Res.,* **124**(8), 8147–8166.

Carcione, J.M., Wang, Z.W., Ling, W., Salusti, E., Ba, J. & Fu, L.Y., 2018. Simulation of wave propagation in linear thermoelastic media, *Geophysics,* **84,** T1–T11.

Cermak, V., Bodri, L., Rybach, L. & Buntebarth, G., 1990. Relationship between seismic velocity and heat production: comparison of two sets of data and test of validity, *Earth planet. Sci. Lett.,* **99**(1–2), 48–57.

Deresiewicz, H., 1957. Plane waves in a thermoelastic solid, *J. acoust. Soc. Am.,* **29,** 204–209.

Eslami, M.R., Hetnarski, R.B., Ignaczak, J., Noda, N., Sumi, N. & Tanigawa, Y., 2013. *Theory of Elasticity and Thermal Stresses,* Vol. **197,** p. 786, Springer.

Fu, L.Y. & Bouchon, M., 2004. Discrete wavenumber solutions to numerical wave propagation in piecewise heterogeneous media—I. Theory of two-dimensional SH case, *Geophys. J. Int.,* **157**(2), 481–498.

Fu, L-Y, 2012. Evaluation of sweet spot and geopressure in Xihu, Sag. Tech Report, CCL2012-SHPS-0018ADM. Key laboratory of petroleum resource research, Institute of Geology and Geophysics, Chinese Academy of Sciences.

Fu, L-Y, 2017. Deep-superdeep oil gas geophysical exploration 111. Program report jointly initiated by MOE and SAFEA, B18055. School of Geosciences China University of Petroleum (East China).

Green, A.E. & Lindsay, K.A., 1972. Thermoelasticity, *J. Elasticity,* **2,** 1–7.

Hu, S.Z., Fu, L.Y. & Pei, Z.L., 2009. A boundary element method for the 2-D wave equation in fluid-saturated porous media, *Chinese J. Geophys. (in Chinese),* **52**(9), 2364–2369.

Jackson, H.E., Walker, C.T. & McNelly, T.F., 1970. Second sound in NaF, *Phys. Rev. Lett.,* **25,** 26.

Jacquey, A.B., Cacace, M., Blöcher, G. & Scheck-Wenderoth, M., 2015. Numerical investigation of thermoelastic effects on fault slip tendency during injection and production of geothermal fluids, *Ener. Proc.,* **76,** 311–320.

Kelder, O. & Smeulders, D.M., 1997. Observation of the Biot slow wave in water-saturated Nivelsteiner sandstone, *Geophysics,* **62**(6), 1794–1796.

Kupradze, V.D., Gegelia, T.G., Basheleishvili, M.O. & Burchuladze, T.V., 1976. *Three-Dimensional Problems of the Mathematical Theory of Elasticity and Thermoelasticity,* North-Holland.

Lord, H.W. & Shulman, Y., 1967. A generalized dynamical theory of thermoelasticity, *J. Mech. Phys. Solids,* **15,** 299–309.

McNelly, T.F., Rogers, S.J., Channin, D.J., Rollefson, R.J., Goubau, W.M., Schmidt, G.E. & Pohl, R.O., 1970. Heat pulses in NaF, onset of second sound, *Phys. Rev. Lett.,* **24,** 100.

Nield, D.A. & Bejan, A, 2006. *Convection in Porous Media,* 3rd ed. Springer.

Noda, N, 1990. Thermal stress problem in a fluid-filled porous circular cylinder, *Z. Angew. Math. Mech.,* **70,** 543–549

Norris, A.N., 1994. Dynamic Green's functions in anisotropic piezoelectric, thermoelastic and poroelastic solids, *Proc. R. Soc., A,* **447,** 175–188.

Nowacki, W., 1975. *Dynamic Problems of Thermoelasticity,* Springer Science & Business Media.

Plona, T.J., 1980, Observation of a second bulk compressional wave in a porous medium at ultrasonic frequencies, *Appl. Phys. Lett.,* **36**(4), 259–261.

Poletto, F., Farina, B. & Carcione, J.M., 2018. Sensitivity of seismic properties to temperature variations in a geothermal reservoir, *Geothermics,* **76,** 149–163.

Ritsema, J., Deuss, A.A., Van Heijst, H.J. & Woodhouse, J.H., 2011. S40RTS: a degree-40 shear-velocity model for the mantle from new Rayleigh wave dispersion, teleseismic traveltime and normal-mode splitting function measurements, *Geophys. J. Int.,* **184**(3), 1223–1236.

Rudgers, A.J., 1990. Analysis of thermoacoustic wave propagation in elastic media, *J. acoust. Soc. Am.,* **88,** 1078–1094.

Scarpetta, E., 1990. On the fundamental solutions in micropolar elasticity with voids, *Acta Mech.,* **82,** 151–158.

Scarpetta, E., Svanadze, M. & Zampoli, V., 2014. Fundamental solutions in the theory of thermoelasticity for solids with double porosity, *J. Thermal Stress.,* **37**(6), 727–748.

Sharma, M.D., 2008. Wave propagation in thermoelastic saturated porous medium, *J. Earth Syst. Sci.,* **117,** 951–958.

Simmons, N.A., Forte, A.M., Boschi, L. & Grand, S.P., 2010. GyPSuM: a joint tomographic model of mantle density and seismic wave speeds, *J. geophys. Res.,* **115**(B12), doi:10.1029/2010JB007631.

Tosaka, N., 1985. The integral equation formulation for boundary-value problems by the coupled system of differential equations (in Japanese), *Japan NCTAM,* 323–324.

Tosaka, N. & Suh, I.G., 1991. Boundary element analysis of dynamic coupled thermoelasticity problems, *Comput. Mech.,* **8,** 331–342.

Treitel, S., 1959. On the Attenuation of small-amplitude plane stress waves in a thermoelastic solid, *J. geophys. Res.,* **64,** 661–665.

Wang, Z.W., Fu, L.Y., Wei, J., Hou, W., Ba, J. & Carcione, J.M., 2019. On the Green function of the Lord–Shulman thermoelasticity equations, *Geophys. J. Int.,* **220**(1), 393–403.

Wei, J. & Fu, L.Y., 2019. Evaluation of the hypersingular boundary integral equation for acoustic wave-propagation simulations, *Geophysics,* **84**(6), A53–A58.

Yang, D., Shen, Y. & Liu, E., 2007. Wave propagation and the frequency domain Green's functions in viscoelastic Biot/squirt (BISQ) media, *Int. J. Solids Struct.,* **44**(14–15), 4784–4794.

Yu, G.X. & Fu, L.Y., 2013. Approximate solutions to the boundary–volume integral equation for wave propagation in piecewise heterogeneous media, *Pure appl. Geophys.,* **170**(11), 1803–1819.

APPENDIX: LIST OF SYMBOLS

σ_{ij}	the stress components of the frame
p_f	pore-fluid pressure
λ, μ	the Lamé constants of the drained matrix
δ_{ij}	Kronecker-delta
ϕ	the porosity
T_0	the reference absolute temperature
T	the increment of temperature over T_0
u_i	the displacement components in the solid phase
U_i	the displacement components of the fluid phase
w_i	the displacement components of the fluid relative to the solid frame
K_s	the solid bulk moduli
K_f	the fluid bulk moduli
β_s	the coefficients of thermal stress for the solid phase
β_f	the coefficients of thermal stress for the fluid phase
γ	the coefficient of heat conduction
C_e	the specific heat capacity
τ	the tortuosity
τ_0	the relaxation time
ρ_s	the solid density
ρ_f	the fluid density
ρ	the composite density
η	Viscosity
χ	Permeability
s_i	the polarizations for the motions of the solid particle
d_i	the polarizations for the motions of the fluid particle
A, B, C	amplitude constants
ω	angular frequency
t	Time
v_c	complex velocity
l_j	the propagation directions
x_j	position components
div	the divergence symbol
Δ	Laplacian operator

Key words

Authors are requested to choose key words from the list below to describe their work. The key words will be printed underneath the summary and are useful for readers and researchers. Key words should be separated by a semi-colon and listed in the order that they appear in this list. An article should contain no more than six key words.

COMPOSITION and PHYSICAL PROPERTIES
Composition and structure of the continental crust
Composition and structure of the core
Composition and structure of the mantle
Composition and structure of the oceanic crust
Composition of the planets
Creep and deformation
Defects
Elasticity and anelasticity
Electrical properties
Equations of state
Fault zone rheology
Fracture and flow
Friction
High-pressure behaviour
Magnetic properties
Microstructure
Permeability and porosity
Phase transitions
Plasticity, diffusion, and creep

GENERAL SUBJECTS
Core
Gas and hydrate systems
Geomechanics
Geomorphology
Glaciology
Heat flow
Hydrogeophysics
Hydrology
Hydrothermal systems
Infrasound
Instrumental noise
Ionosphere/atmosphere interactions
Ionosphere/magnetosphere interactions
Mantle processes
Ocean drilling
Structure of the Earth
Thermochronology
Tsunamis
Ultra-high pressure metamorphism
Ultra-high temperature metamorphism

GEODESY and GRAVITY
Acoustic-gravity waves
Earth rotation variations
Geodetic instrumentation
Geopotential theory
Global change from geodesy
Gravity anomalies and Earth structure
Loading of the Earth
Lunar and planetary geodesy and gravity
Plate motions
Radar interferometry
Reference systems
Satellite geodesy
Satellite gravity
Sea level change
Seismic cycle
Space geodetic surveys
Tides and planetary waves
Time variable gravity
Transient deformation

GEOGRAPHIC LOCATION
Africa
Antarctica
Arctic region
Asia
Atlantic Ocean
Australia
Europe
Indian Ocean
Japan
New Zealand
North America
Pacific Ocean
South America

GEOMAGNETISM and ELECTROMAGNETISM
Archaeomagnetism
Biogenic magnetic minerals
Controlled source electromagnetics (CSEM)
Dynamo: theories and simulations
Electrical anisotropy
Electrical resistivity tomography (ERT)
Electromagnetic theory
Environmental magnetism
Geomagnetic excursions
Geomagnetic induction
Ground penetrating radar
Magnetic anomalies: modelling and interpretation
Magnetic fabrics and anisotropy
Magnetic field variations through time
Magnetic mineralogy and petrology
Magnetostratigraphy
Magnetotellurics
Marine electromagnetics
Marine magnetics and palaeomagnetics
Non-linear electromagnetics
Palaeointensity
Palaeomagnetic secular variation
Palaeomagnetism
Rapid time variations
Remagnetization
Reversals: process, time scale, magnetostratigraphy
Rock and mineral magnetism
Satellite magnetics

GEOPHYSICAL METHODS
Downhole methods
Fourier analysis
Fractals and multifractals
Image processing
Instability analysis
Interferometry
Inverse theory
Joint inversion
Neural networks, fuzzy logic
Non-linear differential equations
Numerical approximations and analysis
Numerical modelling
Numerical solutions
Persistence, memory, correlations, clustering
Probabilistic forecasting
Probability distributions
Self-organization
Spatial analysis
Statistical methods
Thermobarometry
Time-series analysis
Tomography
Waveform inversion
Wavelet transform

PLANETS
Planetary interiors
Planetary volcanism

SEISMOLOGY
Acoustic properties
Body waves
Coda waves
Computational seismology
Controlled source seismology
Crustal imaging
Earthquake dynamics
Earthquake early warning
Earthquake ground motions
Earthquake hazards
Earthquake interaction, forecasting, and prediction
Earthquake monitoring and test-ban treaty verification
Earthquake source observations
Guided waves
Induced seismicity
Interface waves
Palaeoseismology
Rheology and friction of fault zones
Rotational seismology
Seismic anisotropy
Seismic attenuation
Seismic instruments
Seismic interferometry
Seismicity and tectonics
Seismic noise
Seismic tomography
Site effects
Statistical seismology
Surface waves and free oscillations
Theoretical seismology

Tsunami warning
Volcano seismology
Wave propagation
Wave scattering and diffraction

TECTONOPHYSICS
Backarc basin processes
Continental margins: convergent
Continental margins: divergent
Continental margins: transform
Continental neotectonics
Continental tectonics: compressional
Continental tectonics: extensional
Continental tectonics: strike-slip and transform
Cratons
Crustal structure
Diapirism
Dynamics: convection currents, and mantle plumes
Dynamics: gravity and tectonics
Dynamics: seismotectonics
Dynamics and mechanics of faulting
Dynamics of lithosphere and mantle
Folds and folding
Fractures, faults, and high strain deformation zones
Heat generation and transport
Hotspots
Impact phenomena
Intra-plate processes
Kinematics of crustal and mantle deformation
Large igneous provinces
Lithospheric flexure
Mechanics, theory, and modelling
Microstructures
Mid-ocean ridge processes
Neotectonics
Obduction tectonics
Oceanic hotspots and intraplate volcanism
Oceanic plateaus and microcontinents
Oceanic transform and fracture zone processes
Paleoseismology
Planetary tectonics
Rheology: crust and lithosphere
Rheology: mantle
Rheology and friction of fault zones
Sedimentary basin processes
Subduction zone processes
Submarine landslides
Submarine tectonics and volcanism
Tectonics and climatic interactions
Tectonics and landscape evolution
Transform faults
Volcanic arc processes

VOLCANOLOGY
Atmospheric effects (volcano)
Calderas
Effusive volcanism
Eruption mechanisms and flow emplacement
Experimental volcanism
Explosive volcanism
Lava rheology and morphology
Magma chamber processes
Magma genesis and partial melting
Magma migration and fragmentation
Mud volcanism
Physics and chemistry of magma bodies
Physics of magma and magma bodies
Planetary volcanism
Pluton emplacement
Remote sensing of volcanoes
Subaqueous volcanism
Tephrochronology
Volcanic gases
Volcanic hazards and risks
Volcaniclastic deposits
Volcano/climate interactions
Volcano monitoring
Volcano seismology